Analyst

ROYAL SOCIETY OF CHEMISTRY

PAPER

View Article Online
View Journal | View Issue

Cite this: *Analyst*, 2021, **146**, 2679

A highly sensitive electrochemical microRNA-21 biosensor based on intercalating methylene blue signal amplification and a highly dispersed gold nanoparticles/graphene/polypyrrole composite

Chammari Pothipor,[a,b,c] Noppadol Aroonyadet,†[d] Suwussa Bamrungsap,[d] Jaroon Jakmunee[a,c,e] and Kontad Ounnunkad *[a,c,e,f]

Numerous clinical studies suggest that microRNAs (miRNAs) are indicative biomolecules for the early diagnosis of cancer. This work aims to develop a cost-effective and label-free electrochemical biosensor to detect miRNA-21, a biomarker of breast cancer. An electrochemical sensor is fabricated using a nanocomposite, consisting of graphene (GP), polypyrrole (PPY) and gold nanoparticles (AuNPs), modified onto a screen-printed carbon electrode (SPCE) to improve electron transfer properties and increase the degree of methylene blue (MB) intercalation for signal amplification. The GP/PPY-modified electrode offers good electrochemical reactivity and high dispersibility of AuNPs, resulting in excellent sensor performance. Peak current of the MB redox process, which is proportional to miRNA-21 concentration on the electrode surface, is monitored by differential pulse voltammetry (DPV). Under optimal conditions, this sensor is operated by monitoring the MB signal response due to the amount of hybridization products between miRNA-21 target molecules and DNA-21 probes immobilized on the electrode. The proposed biosensor reveals a linear range from 1.0 fM to 1.0 nM with a low detection limit of 0.020 fM. In addition, the miRNA-21 biosensor provides good selectivity, high stability, and satisfactory reproducibility, which shows promising potential in clinical research and diagnostic applications.

Received 19th January 2021,
Accepted 15th February 2021

DOI: 10.1039/d1an00116g

rsc.li/analyst

Introduction

MiRNAs are non-coding RNAs that regulate various biochemical processes.[1,2] The miRNAs are released by various kinds of malignant cells, and the irregular expression of specific miRNAs can be applicable for tumor classification.[3] Recent studies show a relationship between changes in miRNA levels with different kinds of cancers.[4–7] The assay of miRNAs as biomarkers is important for early screening of cancer, identifying the cancer type, estimating the stage of cancer, and monitoring the response of cancer treatment.[8–10] Therefore, ultra-trace analysis of miRNA levels relevant to early-stage cancer is the key to improve prognosis. Due to the high stability of miRNAs in human body fluids, they are detectable in plasma, serum, whole blood, and sputum. Therefore, it is proper to use miRNAs as potentially indicative biomarkers for early detection of cancer.[11] Among many miRNAs, miRNA-21 is one of the best-known tumor markers, and its over-expressed level is associated with hepatocellular carcinoma, lung adenocarcinoma and breast cancer.[13–15] Many attempts have been made to develop highly sensitive and selective methods for its assay.[12–16] Besides the DNA microarray assay, DNA sequencing and polymerase chain reaction (PCR) techniques are widely used for the detection of biomarkers from breast cancer.[17–19] However, they relate to multi-step operations, long-time assay, and expensive tools, which significantly limits their applicability for point of care diagnosis. Consequently, inexpensive and quantitative devices with simple operation and fast response to biomarkers at distinct biomolecular levels are developed using electrochemical techniques.[20,21] The detection of miRNAs by electrochemical DNA biosensors associates with the measurement of the change in signal resulting from the capturing process of the complementary miRNA target.[22,23] To evaluate the hybridization process of the DNA

[a]*Department of Chemistry, Faculty of Science, Chiang Mai University, Chiang Mai 50200, Thailand. E-mail: suriyacmu@yahoo.com, kontad.ounnunkad@cmu.ac.th*
[b]*The Graduate School, Chiang Mai University, Chiang Mai, 50200, Thailand*
[c]*Center of Excellence for Innovation in Chemistry, Faculty of Science, Chiang Mai University, Chiang Mai, 50200, Thailand*
[d]*National Nanotechnology Center (NANOTEC), National Science and Technology Development Agency (NSTDA), Pathum Thani 12120, Thailand*
[e]*Research Center on Chemistry for Development of Health Promoting Products from Northern Resources, Chiang Mai University, Chiang Mai, 50200, Thailand*
[f]*Center of Excellence in Materials Science and Technology, Chiang Mai University, Chiang Mai 50200, Thailand*
† Deceased.

probe and complementary miRNA target, either an electrochemical labeling strategy or a label-free method is employed. The label-free electrochemical sensing of miRNA-21 is operated *via* direct detection of the hybridization process with a DNA probe. This biosensor has remarkably become a great analytical tool for the detection of the nucleotide molecule because of its easy preparation, rapid detection, high sensitivity, and low cost.[24–26] Methylene blue (MB) as an electrochemical indicator has been widely used in the detection of nucleic acid hybridization.[27–29] The behavior of MB intercalated to single- and double-stranded oligonucleotides has been studied by electrochemical techniques.[30]

Nanomaterials with good mechanical, physical, and chemical properties have been developed and employed for the construction of biosensing platforms.[31] Several kinds of nanomaterials such as noble metal nanoparticles (NPs), magnetic NPs, conducting polymers, and carbon-based nanomaterials have been studied for improving the sensitivity of electrochemical biosensors. Among these nanomaterials, graphene (GP) and its composites can be employed to construct high-performance electrochemical sensors due to their good electronic transport property and large surface area.[32] GP on the surface of the electrode can enhance the electrochemical sensitivity by increasing the surface area of the platforms and accelerating the electron transfer.[33] The influence of a conductive polymer on the electrode surface conductivity for miRNA detection has been reported.[34] Polypyrrole (PPY) is one of the widely used conductive polymers which can be prepared chemically or electrochemically.[35–38] PPY has attracted great interest in electrochemical sensing applications due to its inherent features, including low-cost preparation, tunable conductivity, and outstanding stability.[39] In addition to the above advantages of the PPY, its surface morphologies, physical properties, and charge characteristics can be modified easily by using different materials.[40–42] Therefore, it is believed that the application of both PPY and GP can enhance the electrochemical properties of the biosensing platform. In addition, using nanomaterials can increase the long-term stability of biosensors due to their unique properties.[43] AuNPs have attracted much attention in the electrochemical analysis due to their excellent physical and chemical properties, such as good electrical properties, strong adsorption ability, and good surface properties.[44–48] Moreover, AuNPs are biocompatible and can be anchored on various kinds of surfaces. AuNPs have been used as supports for immobilizing the active biomolecules, such as proteins, enzymes, antibodies, and nucleic acids.[49] Therefore, AuNPs have been intensively used to fabricate a variety of electrochemical sensors by their modification on sensing surfaces.[50–53]

Herein, a highly selective and sensitive electrochemical biosensor is developed to detect miRNA-21 using a capture DNA-21 probe-AuNP conjugates/GP/PPY modified SPCE. MB is used as a signaling molecule, and GP and PPY are used as signal-enhancing materials. Moreover, AuNPs are well-dispersed on PPY particles and the GP/PPY composite that can cause high distribution of the DNA probe on the sensing surface. This good biosensor interface offers high device sensitivity. A thiol linked DNA probe specifically designed for hybridization with miRNA-21 is functionalized on AuNPs, which are deposited on the GP/PPY modified SPCE surface. Then, the hybridization process between the DNA probe and its miRNA target occurs at the electrode surface, thereafter, allowing an increase in the attachment of MB. Each modification and immobilization step are monitored by electrochemical techniques. We observe satisfactory reproducibility and stability in detecting miRNA-21. Our biosensor also offers high sensitivity and selectivity and is applicable for the detection of miRNA-21 in human serum samples.

Experimental section

Chemicals and reagents

Phosphate buffered saline tablets (PBS), potassium chloride (KCl, 99.0%), 6-mercapto-1-hexanol (MCH, 97.0%), trisodium citrate dihydrate ($Na_3C_6H_5O_7$, 99.0%), iron(III) chloride ($FeCl_3$, 99.0%), gold(III) chloride trihydrate ($HAuCl_4{\cdot}3H_2O$, ≥99.9%), methylene blue (MB, >97.0) and human serum from a human male (AB plasma, USA origin, product number: H4522, lot: SLBS6544) were purchased from Sigma Aldrich (USA). Potassium nitrate (KNO_3, 99.0%), sulfuric acid (H_2SO_4, 96.0%), potassium permanganate ($KMnO_4$, 99.0%), hydrochloric acid (HCl, 37.0%), sodium nitrate ($NaNO_3$, 99.0%), sodium chloride (NaCl, >99.5%), synthetic graphite powder <20 micron, potassium ferricyanide ($K_3Fe(CN)_6$, 98.5%) and potassium ferrocyanide ($K_4Fe(CN)_6$, 98.5%) were obtained from Merck (Germany). Hydrogen peroxide (H_2O_2, 50.0%) was purchased from Carlo Erba Reagent, (Italy). Pyrrole monomer (99%), Tris(2-carboxyethyl) phosphine hydrochloride (TCEP-HCl) and 10 mM Tris (hydroxymethyl)-HCl (Tris-HCl) containing 1.0 mM ethylenediaminetetraacetic acid (EDTA) were obtained from Fisher Scientific (USA). Screen printed carbon electrodes (SPCEs) were obtained from Zensor Research and Development (USA). All oligonucleotides used in this research were purchased from Tech Dragon Ltd Company (Hong Kong) and their sequences are listed in Table 1. The glassware used in the preparation and storage of AuNPs was cleaned with aqua regia solution (3 : 1 of $HCl : HNO_3$), washed with DI water, and dried in an oven at 60 °C. All glassware and microtips were autoclaved to

Table 1 The sequences of nucleic acids used in this research

Name of oligonucleotides	Sequence (5′ to 3′)
Capture DNA probe	TCAACATCAGTCTGATAAGCTATTT-Thiol
miRNA-21	UAGCUUAUCAGACUGAUGUUGA
Single-base mismatch miRNA-21 (1MT-miRNA-21)	UAGCUUAUCGGACUGAUGUUGA
Triple-base mismatch miRNA-21 (3MT-miRNA-21)	UUGCUUAUCGGACUGAUCUUGA
Non-complementary miRNA-21	GUAAUGCAUCUGACCGAAGGCA
miRNA-155	UUAAUGCUAAUCGUGAUAGGGG

eliminate the influence of DNases and RNases on the stability of the DNA probe and miRNAs.

Instrumental

Differential pulse voltammetry (DPV) and cyclic voltammetry (CV) measurements were performed with an Emstat 3 (Plamsens, Netherlands) controlled by PSTrace 5.6 software. The electrochemical impedance spectroscopy (EIS) measurement was carried out using an Autolab potentiostat/galvanostat (Metrohm, Netherlands) dictated by NOVA 2.1 software.

The electrochemical measurements were performed using three-electrode system SPCEs. A high speed centrifuge (5430R Eppendorf, Germany) was used for the purification of the AuNP solution. A thermomixer (ThermoMixer C, Eppendorf, Germany) was employed for mixing and incubating bioconjugated samples. The morphologies of the nanomaterials were characterized by scanning electron microscopy (SEM, JEOL JSM-6335F, Japan) and transmission electron microscopy (TEM, JEOL JEM 210, Japan). The absorption spectrum of the AuNP solution was obtained using an ultraviolet–visible-near-infrared (UV–Visible-NIR) spectrophotometer (Power Wave XS2, Bio-Tex, USA). A size distribution histogram was measured using a DLS Nano Sizer (Malvern Instruments, UK).

Synthesis of AuNPs and adsorption of the single strand-DNA (ss-DNA) probe to AuNPs

The AuNPs were prepared following a previous report.[54] Briefly, 50 mL of 1.0 mM $HAuCl_4{\cdot}3H_2O$ solution was stirred vigorously in a round bottom flask. Next, the gold solution was heated at 100 °C and then 5.0 mL of 38.8 mM $Na_3C_6H_5O_7$ aqueous solution was added with rapid mixing. After heating for 20 min, the obtained solution was cooled at room temperature under stirring. The AuNP solution was subsequently purified by centrifugation at 6000 rpm for 10 minutes at 25 °C. The final product was re-dispersed in sterile water and then kept at 4 °C for further use.

For the adsorption of the ss-DNA probe to AuNPs, 10 μL of 0.2 mM TCEP-HCl in 10 mM of tris-EDTA and 10 μL of 20 μM capture DNA were mixed in a thermomixer at 400 rpm for 2 h to break S–S bonds of the capture DNA probe for functionalization of AuNPs. Then, 50 μL of AuNP solution (O.D. = 1) was mixed with 5.0 μL of 10 μM capture DNA probe solution. After that, 50 μL of 0.10 mM PBS containing 0.20 mM NaCl was added for 1 h. Finally, the resultant product was washed by centrifugation at 5500 rpm for 10 min at 25 °C 3 times and then was dispersed and adjusted to 50 μL with PBS solution.

Preparation of GP, PPY and the GP/PPY composite

GP was synthesized by the modified Hummers' method. 0.20 g of graphite powder was mixed with 36.0 mL of 96.0% w/v H_2SO_4 and 24 mL of 65.0% w/v HNO_3. The mixture was stirred for 1 h, and then 0.10 g of $NaNO_3$ was added under stirring for 20 min in an iced bath. A portion of 0.60 g $KMnO_4$ was added into the mixture and stirred for 1 hour. After that, 6.0 mL of DI water was added and stirred for 30 min. Additional 0.60 g of $KMnO_4$ was put into the solution and stirred for 1 h. The mixture was diluted with 100 mL of DI water and stirred overnight at room temperature. After that, 2.0 mL of 30% v/v H_2O_2 was dropped into the solution. The GO was washed with DI water several times by centrifugation at 9000 rpm for 25 min. The solution was dried in an oven at 70 °C.[55,56] To reduce GO to GP, 5.0 mg GO powder was dissolved in 5.0 mL of DI water to obtain a concentration of 5 mg mL^{-1}, under sonication for 30 min and 0.50 mL of 10% v/v hydrazine was added. The solution was heated at 100 °C for 1 h until the color change from brown to black.[57]

The PPY was prepared by the chemical oxidation polymerization.[58] Briefly, 1.42 mL of 8.75 mmol $FeCl_3$ solution (oxidant for PPY synthesis) was diluted in 50 mL of 1.0 M HCl under cooling and stirring for 30 min. Then, 1.22 mL of 17.56 mmol pyrrole monomer was injected into the solution. After 30 min, the mixture was filtered. The PPY was sequentially rinsed with methanol and acetone. The final product was dried in an oven at 40 °C for 16 h. For the preparation of the electrode modifier solution, 1.0 mg mL^{-1} GP/PPY composite is dissolved in a water–isopropanol mixture (9 : 1) solution and sonicated for 30 min. The ratios of GP and PPY used in this study are 10 : 90, 20 : 80, 30 : 70, 40 : 60, 50 : 50, 60 : 40, 70 : 30, 80 : 20 and 90 : 10.

Preparation of the electrochemical miRNA-21 biosensor

The schematic of the preparation of a label-free electrochemical miRNA-21 biosensor is shown in Fig. 1. Firstly, 5.0 μL of each GP/PPY solution (0 : 100, 10 : 90, 20 : 80, 30 : 70, 40 : 60, 50 : 50, 60 : 40, 70 : 30, 80 : 20, 90 : 10, or 100 : 0) was dropped onto the SPCE. The GP/PPY-modified SPCE (GP/PPY/

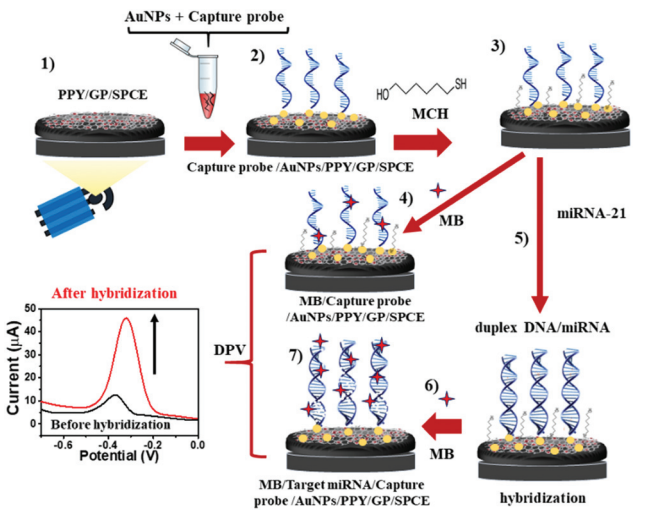

Fig. 1 Schematic of various steps of biosensor fabrication and miRNA detection; (1) modification of the GP/PPY composite on a surface of the SPCE; (2) deposition of adsorbed ss-DNA-21 probe/AuNPs on a modified electrode; (3) adding MCH blocking solution; (4) adsorption of MB into capture DNA-21/AuNPs/GP/PPY/SPCE; (5) capturing the miRNA-21 target at the DNA-21 probe; (6) adsorption of MB into miRNA-21/capture DNA-21/AuNPs/GP/PPY/SPCE; (7) recording DPV responses of the electrodes before and after hybridization.

SPCE) was dried at room temperature. Accordingly, 10.0 μL of capture DNA-21/AuNP solution was drop-cast onto the GP/PPY/SPCE and the electrode was dried at room temperature. Then, the electrode surface was blocked with 10 μL of 2 mM MCH solution for 1 h and washed with DI water. Before incubation with the target solution, the electrode modified with capture DNA-21/AuNPs/GP/PPY/SPCE was immersed in 5.0 μL of 40 μM MB solution for 5 min. Then, the DPV response was recorded as a baseline response after the electrode was rinsed with PBS several times. After that, the capture DNA-21 probe-immobilized electrode was incubated in 1.0× SSC containing the target miRNA-21 for 1 h to achieve the hybridization process. The non-hybridization miRNA-21 was eliminated from the biosensor surface by washing with 0.1 × SSC. Then, the miRNA-21/capture DNA-21/AuNPs/GP/PPY/SPCE was immersed in 5.0 μL of 40 μM MB solution for 5 min. The excess MB was washed with PBS solution to ensure that the obtained current signal was only caused by MB bounding the duplex structure formed. Finally, the electrochemical signal of MB was estimated with the DPV technique in 10 mM PBS at pH 7.4.

Results and discussion

Characterization of the materials

The morphology of AuNPs was characterized by SEM and TEM techniques. As seen in Fig. 2, the SEM (a) and TEM (b) images of AuNPs reveal almost a uniform size and spherical shape.

In addition, the AuNP solution was also characterized using a UV-Vis-NIR spectrophotometer and a DLS Nano Sizer. The AuNP solution exhibits an absorption peak at 510 nm (Fig. 2(c)) and the resulting AuNPs have an average diameter of 29.46 ± 1.18 nm (Fig. 2(d)).

The surface morphologies of the unmodified and modified electrodes were studied by the SEM technique. In Fig. 3(a), the SPCE surface exhibits fragments of carbon particles that make up the cavity, typically with high roughness. After the SPCE is modified with GP sheets (Fig. 3(b)), the surface is covered with a crumbled film and a tissue-like structure of GP. Moreover, the PPY film on the SPCE has a cauliflower-like structure (Fig. 3(c)). When the GP/PPY nanocomposite is dropped onto the surface of the electrode (Fig. 3(d)), sheet-like GP is inserted into the PPY structure. After that, the capture DNA probe-functionalized AuNPs are deposited on the above bare SPCE, GP/SPCE, PPY/SPCE, and GP/PPY/SPCE (Fig. 3(e–h), respectively). It is clearly observed that AuNPs are highly distributed on the surfaces of PPY and the GP/PPY nanocomposite. The particle agglomerates are found after the deposition of AuNPs on a bare SPCE and GP. The increment amount of the PPY on the surface not only increases the active surface area, but also improves the dispersibility of AuNPs onto the electrode surface, as shown in Fig. 3(g–h). The good biocompatibility and high dispersibility of AuNPs can enhance the amount of immobilized DNA probes and give proper orientation of the DNA probes. Moreover, the high conductivity of AuNPs can improve the electron transfer rate of the sensor. From these reasons, using AuNPs would result in good device performances, especially high sensitivity and selectivity.

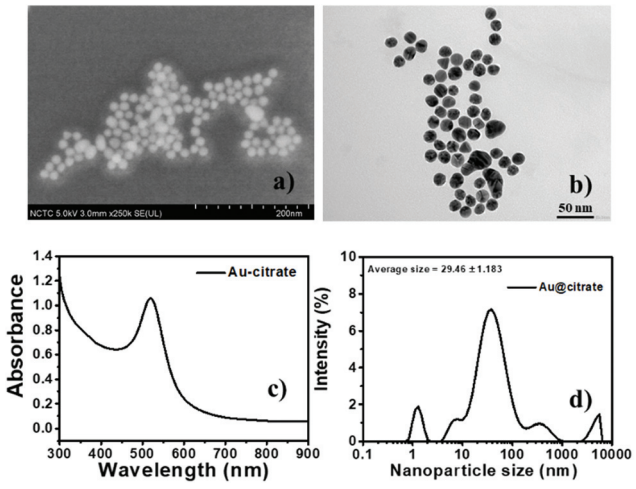

Fig. 2 (a) SEM image of the AuNPs, (b) TEM image of AuNPs, (c) UV-Vis absorbance spectrum of AuNPs and (d) size distribution histogram of AuNPs.

Electrochemical characterization of the different modified electrodes

In general, CV is used for the study of an electrochemical process at the electrode/solution interface. The measurement is carried out on the corresponding electrodes in contact with 0.10 M KCl solution containing 5.0 mM $[Fe(CN)_6]^{3-/4-}$ in the potential range from −0.4 V to +0.8 V at a scan rate of 50 mV s^{-1}. The electrodes show differences in the current response values and distinct peak-to-peak separations ($\Delta E_p = E_{pa} - E_{pc}$). A couple of well-defined reversible redox peaks of $[Fe(CN)_6]^{3-/4-}$ are observed at all electrodes (Fig. 4(a)). The oxidation peak current increases to 98.53 μA, and ΔE_p decreases to 0.203 V when the SPCE is modified with GP (red line), implying the promotion of faster electron transfer. It is attributed to the high surface area and high conductivity of the GP.[43,59] By the modification with PPY (Fig. 4, blue curve), the peak current sharply increases to 111.0 μA, and a slight decrease in the ΔE_p value (0.177 V) is observed. High peak current results from the higher surface area and higher electrochemical reactivity of PPY. Moreover, the GP/PPY-modified SPCE shows that the peak current increases to 114.2 μA and ΔE_p significantly decreased to 0.175 V (Fig. 4, pink curve). This behavior results from the synergetic effect of GP and PPY.

Moreover, the EIS technique is used to characterize the modified electrodes. As presented in Fig. 4(b), the unmodified SPCE provides a small semicircle indicating the highest electron-transfer resistance (R_{et}) of approximately 1.474 kΩ (black curve). When the GP, PPY, and GP/PPY nanocomposites are deposited on the surface of the SPCE, these impedance values are further decreased as compared with that of the SPCE, and the electrodes display an almost straight line (red, blue, and pink line, respectively), implying that these materials behave

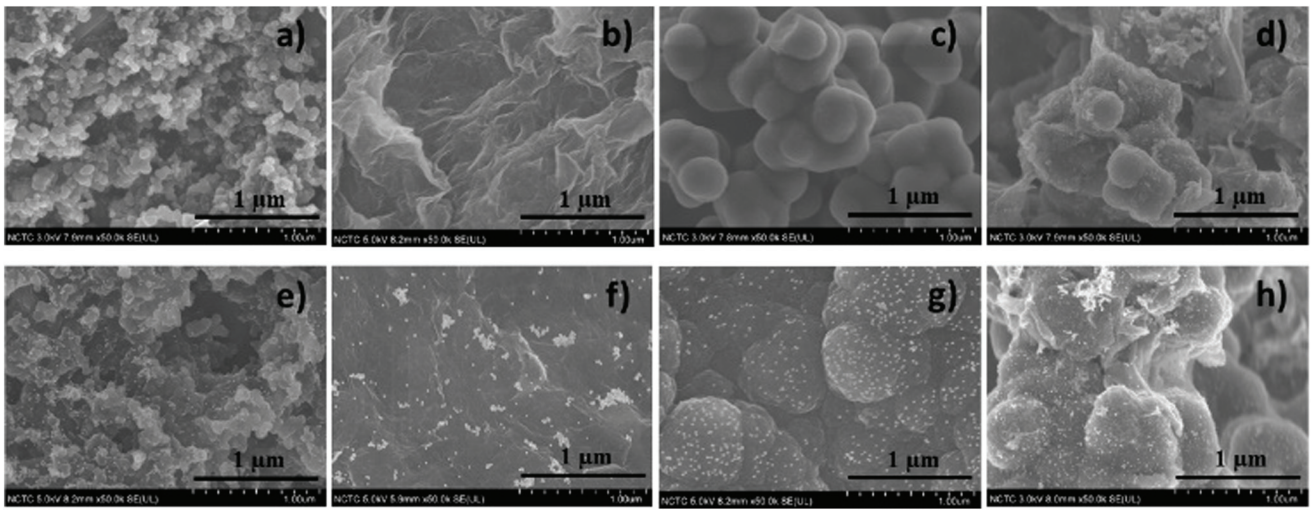

Fig. 3 SEM images of (a) bare SPCE, (b) GP/SPCE, (c) PPY/SPCE, (d) GP/PPY/SPCE, (e) capture DNA-21-AuNPs/SPCE, (f) capture DNA-21-AuNPs/GP/SPCE, (g) capture DNA-21-AuNPs/PPY/SPCE and (h) capture DNA-21-AuNPs/GP/PPY/SPCE.

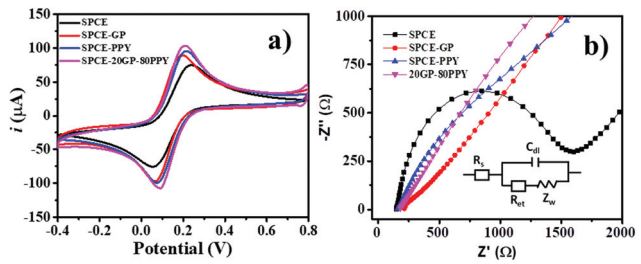

Fig. 4 (a) CVs of bare and modified SPCEs in contact with 0.10 M KCl containing 5.0 mM $[Fe(CN)_6]^{3-/4-}$ at a scan rate of 20 mV s^{-1}. (b) EIS spectra of bare and modified SPCEs in contact with 0.10 M KCl containing 5.0 mM $[Fe(CN)_6]^{3-/4-}$ in the frequency range from 0.1 Hz to 10 kHz and amplitude of 0.010 V.

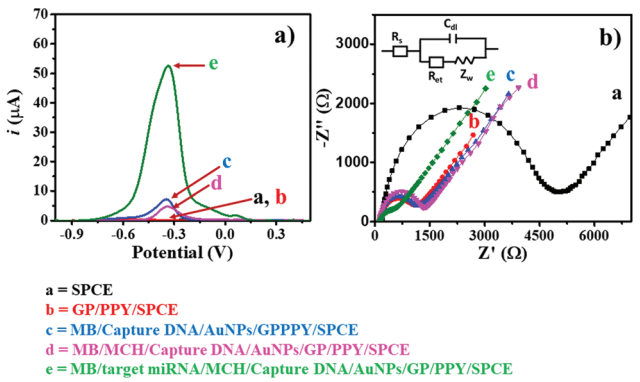

Fig. 5 (a) DPV responses of the bare and modified SPCEs in contact with 0.010 M PBS (pH 7.4). The potential was scanned from −1.0 to 0.5 V; amplitude: 0.05 V, pulse width: 0.02 s and scan rate: 0.01 V s^{-1}. (b) EIS responses of bare and modified SPCEs in contact with 0.010 M PBS (pH 7.4) containing 5.0 mM $[Fe(CN)_6]^{3-/4-}$ in the frequency range from 0.1 Hz to 10 kHz and amplitude of 0.010 V.

as conductors.[60,61] Therefore, all materials modified on the electrode can facilitate the electron transfer.

According to both electrochemical characterization studies, the change of R_{et} in the EIS result is consistent with CV, confirming the successful modification process. Although all materials can reduce the R_{et} value, the GP/PPY-modified SPCE exhibits the highest peak current, thus giving the high sensitivity of sensors. Furthermore, the redox response of the attached MB would be improved by this electrode.

Fabrication of the biosensor

To monitor each step of the biosensor construction, DPV and EIS measurements had been carried out. Fig. 5 shows the DPV curves of various modified electrodes from each step in 0.010 M PBS (pH 7.4) in the potential range from −1.0 to 0.5 V. No distinct redox peaks are observed at the SPCE electrode ((Fig. 5(a), curve a) and GP-PPY modified SPCE (Fig. 5(a), curve b)). A redox peak of MB at 0.35 V is seen with 7.01 μA (Fig. 5(a), curve c), indicating that the MB is attached to the capture DNA probe on AuNPs/GP/PPY/SPCE surface by the electrostatic interaction (Fig. 5(a), curve c). The amount of MB adsorbed on this electrode, which is calculated by area under the oxidation peak of CV, is 11.24 pmole (3.60 ng). Then, the surface of the capture DNA-21/AuNPs/GP/PPY/SPCE is blocked with MCH solution, as found with the declined redox peak current of 4.36 μA (Fig. 5(a), curve d). After the capture DNA-21 on the electrode hybridizes with target miRNA-21 (100 pM), the peak current increases to 52.12 μA (Fig. 5(a), curve e). The increase in the electrochemical response indicates higher amounts of MB molecules intercalating into a duplex (ssDNA/miRNA-21 hybrid) on the electrode surface.[3,30] The MB uptake in the duplex on the electrode is 30.16 pmole (9.65 ng, 168% increase in response). The possible mechanisms of the MB intercalation involve its affinity with guanine base (G) on DNA. The strong affinity is based on the electrostatic interaction

between positive charge of MB and the negative charge from the phosphate backbone of the DNA structure.[62–64]

In addition, EIS spectra in PBS (pH 7.4) solution with the presence of 5.0 mM $[Fe(CN)_6]^{3-/4-}$ also confirm each successful fabrication step of the biosensor. The SPCE has the biggest semicircle with R_{et} of 4.535 kΩ (Fig. 5(b) curve (a)). The R_{et} value decreases to 1.095 kΩ after the SPCE is modified with GP/PPY. When MB molecules are immobilized onto the capture DNA-21 probe/AuNPs/GP/PPY/SPCE, the R_{et} is 1.092 kΩ (Fig. 5(b) curve (c)). The R_{et} slightly increases to 1.197 kΩ when the electrode is incubated with MCH solution. A higher R_{et} is caused by the blocking with non-conducting MCH molecules (Fig. 5(b) curve (d)). Subsequently, after the miRNA-21 target is captured by the DNA probe to form double-strand complexes, the R_{et} value again decreases to 0.920 kΩ (Fig. 5(b) curve (e)), indicating that the electron transfer of $[Fe(CN)_6]^{3-/4-}$ is improved. In this case, the strength of negative charge on immobilized DNA is lowered by hybridization with miRNA-21 and attachment of positively charged MB. This governs the better mass transfer of $[Fe(CN)_6]^{3-/4-}$ into the electrode due to lower repulsion force. It is evident that the miRNA-21 sensor has been successfully developed.

Optimization of the experimental conditions

Several crucial sensing parameters, including electrode material composition (GP : PPY), PBS concentration, immobilization time of the DNA-21 probe, hybridization time, concentration of the MB redox probe for signal generation, and adsorption time of MB for signal generation, play important roles in sensing performances as shown in Fig. 6 and 7. In this work, DPV is used to evaluate the parameters' influence on the properties of the fabricated biosensor. All these variables are optimized by comparing the difference between the oxidation peak currents (Δi) of MB measured before and after hybridization with 100 pM miRNA-21.

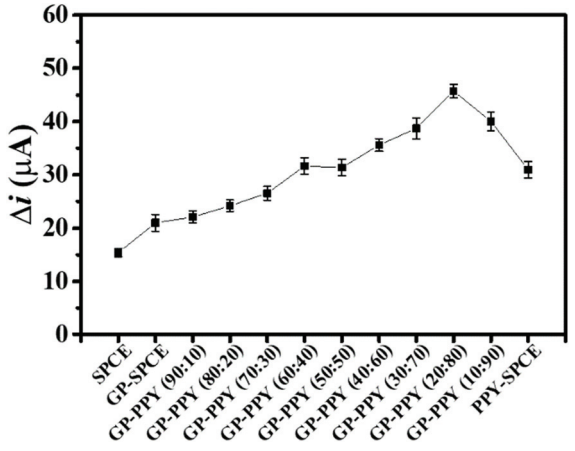

Fig. 6 Current responses for the detection of 100 pM miRNA-21 by biosensors based on bare SPCE, GP, PPY and GP/PPY composites with different ratios (90 : 10, 80 : 20, 70 : 30, 60 : 40, 50 : 50, 40 : 60, 30 : 70, 20 : 80 and 10 : 90).

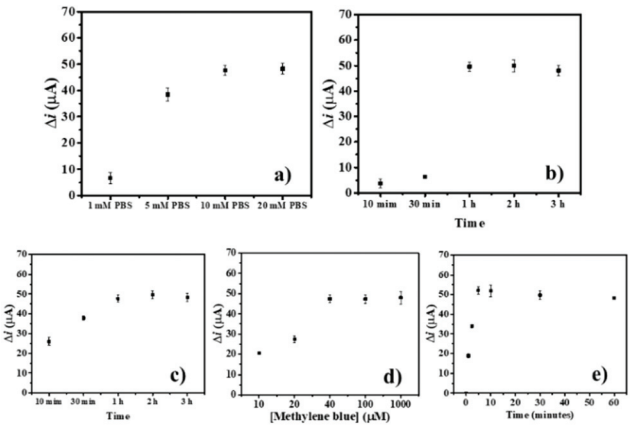

Fig. 7 Optimization of experimental parameters. (a) The PBS concentration, (b) the immobilization time of the DNA-21 probe, (c) the hybridization time, and (d) the MB redox probe concentration and (e) the adsorption time of MB for signal generation.

Each ratio of GP and PPY in the composite is investigated to obtain the best signal amplification for the detection of 100 pM miRNA-21 by the developed biosensor (Fig. 6). After the amount PPY in the ratio of GP : PPY increases, the Δi of the peak currents of MB before and after hybridization increases. The best sensitivity of the constructed biosensor is achieved when the SPCE is modified by the composite with a GP : PPY ratio of 20 : 80. Therefore, the electrode modified with this ratio is chosen throughout the present work. In addition, the effect of the PBS concentration (pH 7.4) on the electrochemical response is firstly investigated after hybridization. The responses of MB in a series of PBS concentrations (1.0, 5.0, 10, and 20 mM) are measured. It is observed that the electrochemical response of the biosensor is obviously changed with different PBS concentrations (Fig. 7(a)). This might result from the variation of chemical properties of the biosensor by the change of ionic strength of the electrolyte. The signal difference (Δi) increases as the PBS concentrations increase from 1.0 to 10 mM and remains constant upon increasing PBS concentration to 20 mM. Therefore, 10 mM PBS is selected as the electrolyte solution. The degree of hybridization generally depends on the suitable orientation and the amount of DNA probes on AuNPs as well as on the sensing surface. The increase in the oxidation peak current of MB results from the enhanced amount of the capture DNA probe as well as the amount of the corresponding hybrid formation. Therefore, the probe immobilization time is optimized in order to achieve the saturation of DNA-21 probes on the AuNPs/sensing surface, giving the highest hybridization. Consequently, immobilization time of the capture probe is evaluated in the time range from 10 to 180 min. The result represents that the difference in peak currents (Δi) of MB before and after the hybridization increases to a maximum point at 1 h and remains constant thereafter (Fig. 7(b)), which can imply that the further immobilization of the DNA probe does not occur. Moreover, a limited number of DNA probes as active sites to capture

miRNA-21 on the sensing surface start from 1 h. Thus, 1 h is selected as the optimal incubation time for the capture DNA-21 probe. The hybridization efficiency involves the time of incubation with the target miRNA-21 solution. The influence of miRNA-21 hybridization time on the response redox signal is also investigated in the period of time from 10 to 180 min (Fig. 7(c)). It is shown that the difference of peak currents gradually increases as the capturing time of miRNA-21 increases from 10 to 60 min, and the plateau is observed from 60 min. This indicates that the hybridization of miRNA-21 is completed after 60 min. To achieve high sensitivity of the miRNA-21 detection, hybridization time of 60 min was chosen.

In addition, the effects of MB concentration and absorption time of MB on signal generation due to its intercalation into the DNA/miRNA-21 duplex structure are studied to acquire the best detection sensitivity of the miRNA. To obtain the best response of MB, an increase in the MB concentration from 10 to 1000 μM is applied for detection of 100 pM miRNA-21 as illustrated by Fig. 7(d). The current response of MB due to the hybridization process is significantly raised with increasing the concentration from 10 to 40 μM (Fig. 7(d)). However, the flat curve is found with the concentrations from 40 to 1000 μM. For the first region, the current increase is due to the collective MB intercalating into the hybridization structure. For the second region, the MB cannot further insert the DNA/miRNA-21 duplex structure because the binding sites are limited. Consequently, the optimum MB concentration is achieved at 40 μM. Additionally, the effect of the adsorption time on the analytical signal is shown in Fig. 7(e). The time for MB adsorption is varied from 1 to 60 min. The current difference, caused by the hybridization, is enhanced rapidly with the increment of the absorption time from 1 to 5 min. The insignificant change in the difference value is maintained after 5 min. To maximize the sensitivity and shorten the assay time in the miRNA-21 detection, 5 min is selected as the optimal incubation time for MB adsorption into DNA/miRNA-21 duplex. From the evidence above, the MB concentration of 40 μM and the MB adsorption time of 5 min are employed for the whole experiments.

Analytical performance of the biosensor

After the construction of the capture DNA-21/AuNPs/GP/PPY/SPCE under the optimal conditions, the biosensor efficiency for the detection of miRNA-21 is analyzed by DPV measurements (Fig. 8). It is observed that the DPV peak current of MB noticeably increases when rising the miRNA-21 concentrations in PBS as listed in Fig. 8(a). This results from the improved MB intercalation into the hybridization structure formed by increasing the target miRNA-21 amount. Fig. 8(b) shows that the Δi value linearly increases with increasing the miRNA-21 concentration from 0.001 to 1000 pM. The limit of quantitation (LOQ) and the limit of detection (LOD) are calculated to be 0.66 fM ($10SD_{blank}$ per slope) and 0.020 fM ($3SD_{blank}$ per slope), respectively.

In addition, human serum is employed as a model for the target miRNA-21 detection in the biological matrix. Seven concentrations of miRNA-21 spiked into 50% diluted human serum are tested by the developed biosensor. As seen in Fig. 8(c), the current increases linearly with the concentration of the target miRNA-21. The responses from this study are also employed to construct a calibration curve as presented in Fig. 8(d). It is found that the calibration curves achieved in PBS and serum are not significantly different in terms of analytical response regarding the corresponding target concentration and calibration slope. This suggests that the matrix, namely interfering biological substances, has a negligible effect on the detection of miRNA-21. It is plausible that our proposed biosensor seems to tolerate toward the interferences in human serum.

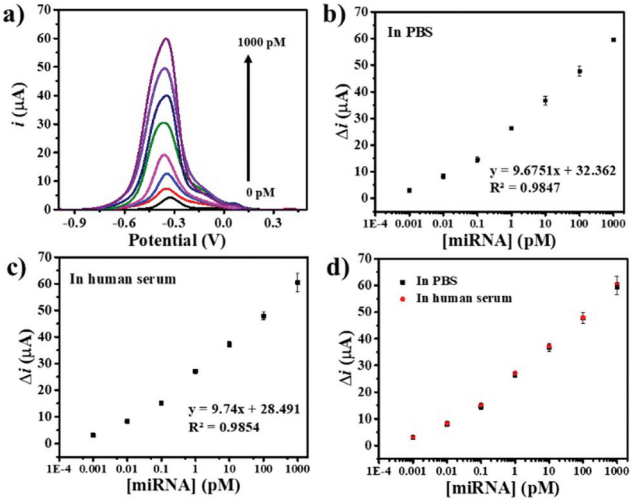

Fig. 8 (a) DPV responses of the miRNA-21 biosensor at different concentrations of miRNA-21 ranging from 0 to 1000 pM, (b) calibration curve of peak current *vs.* miRNA-21 concentration in PBS solution, (c) calibration curve of peak current *vs.* miRNA-21 concentration in human serum, and (d) the comparison of two calibration curves.

Moreover, the resulting percentage of recovery and relative standard deviation (RSD) for the detection of miRNA-21 in seven spiked solutions are calculated, as listed in Table 2. The % recoveries are observed in the range from 98.0% to 108.2% with the % RSD values ranging from 2.69% to 7.78%. The % RSD values are less than 8.0%, suggesting that this biosensor is satisfactory for the determination of miRNA-21 in the complex biological matrix (human serum). Table 3 shows the

Table 2 Determination of the miRNA-21 concentration level in human serum. All measurements were a mean of five replicates (n = 5)

Samples	Added (pM)	Detected (pM)	Recovery (%)	RSD (%)
1	0.001	0.00104	104.0 ± 0.3	7.78
2	0.01	0.00980	98.0 ± 0.4	4.68
3	0.1	0.1068	106.8 ± 0.8	5.05
4	1	1.082	108.2 ± 0.7	2.69
5	10	10.174	101.7 ± 1.1	3.06
6	100	101.6	101.6 ± 1.5	3.02
7	1000	1012.9	101.3 ± 3.4	5.61

Table 3 The comparison of the proposed sensing systems with selected previously published electrochemical biosensors for miRNA-21 detection

Brief biosensing	Applied nanomaterial	Electrode/electrochemical method	Linear range	Detection limit	Ref.
Capture ss-DNA probe/MB[a]	MWCNT-COOH[d]	GCE[h]/DPV[i]	0.1–500 pM	84.3 fM	3
Inosine substituted anti-miRNA 21 probe	Graphite	PGE/DPV	0.17–6.7 μg mL^{-1}	4 pM	69
Capture miRNA 21 probe/MDB[b]	PPY[e]	PGE[j]/EIS[k] & DPV	1.0–10 μg ml^{-1}	0.17 nM	70
Hairpin molecule beacon probe	GP[f]/AuNPs[g]	GCE/Amp[l]	0.1–70 pM	0.06 pM	71
Capture DNA-21 probe/RuHex[c]	AuNPs	SPGE[m]/DPV	100 aM–100 pM	100 aM.	72
Capture DNA-21 probe/MB[a]	AuNPs/GP/PPY	SPCE[n]/DPV	1 fM–1 nM	0.02 fM	This work

[a] Methylene Blue. [b] Meldola's blue. [c] Hexaammineruthenium(III) chloride. [d] Carboxylated multi-wall carbon nanotubes. [e] Polypyrrole. [f] Graphene. [g] Gold nanoparticles. [h] Glassy carbon electrode. [i] Differential pulse voltammetry. [j] Pencil graphite electrode. [k] Electrochemical impedance spectroscopy. [l] Amperometric. [m] Screen-printed three gold electrodes. [n] Screen-printed carbon electrode.

comparison of performance of our sensor with others. As shown in this table, our developed biosensor's detection performance is acceptable and comparable with the other sensors.

Furthermore, the AuNPs/GP/PPY/SPCE-based electrochemical biosensor presents a facile, rapid and cost-effective detection strategy as compared to that using complex multi-step fabrication and enzymes.[65–68] Therefore, this developed biosensor has potential for the detection of miRNA-21 in complex biological samples, making it a good candidate for future clinical applications.

Specificity, reproducibility, and stability of the proposed miRNA biosensor

The selectivity of the proposed miRNA-21 biosensor is an important factor to determine miRNA-21 accurately. Among various miRNAs, the discrimination of the specific sequence of target miRNA-21 from other sequences by our sensor is necessary. The target and other miRNAs having different oligonucleotide sequences, including miRNA-21, single-base mismatch miRNA-21 (1MT-miRNA-21), triple-base mismatch miRNA-21 (3MT-miRNA-21), non-complementary miRNA-21, and miRNA-155, are used in this study. The selectivity of the sensor based on the capture DNA-21/AuNPs/GP/PPY/SPCE is examined in the solution containing each substance. Fig. 9(a) shows the current responses after the probe modified-SPCE is incubated with different miRNAs at a concentration of 100 pM. It is observed that non-targets including 1MT of miRNA-21, 3MT of miRNA-21, non-complementary of miRNA-21, and miRNA-155 yield DPV currents of 5.52, 4.33, 4.57, and 4.48 μA, respectively, similar to the unhybridization. Attractively, the current signal of the complementary miRNA-21 target is nearly 10-fold higher than those of the mismatched miRNA sequences. This result confirms that the proposed biosensor provides high selectivity for the detection of the perfect complementary miRNA-21 target over these interferences as well as others in human serum (see Fig. 8(d)). In addition, it is noted that the complementary miRNA-21 sequences are attached certainly onto the surface of the MCH/capture-DNA-21/AuNPs/GP/PPY film. Moreover, the storage stability of the miRNA-21 biosensor is also evaluated as shown in Fig. 9(b). The sensing platform is kept at 4 °C, when not in use. After five weeks, the redox signal response of the biosensor retains about 83.60% of its initial value. The high stability may be due to a stable DNA-21 capture probe on a MCH/capture-DNA-21/AuNPs/GP/PPY film-modified SPCE. To test the reproducibility of the miRNA-21 sensor, nine modified electrodes are fabricated with the same conditions for electrochemical detection of 100 pM miRNA-21. All modified electrodes show current signals with the % RSD of 3.26. This result indicates that the proposed

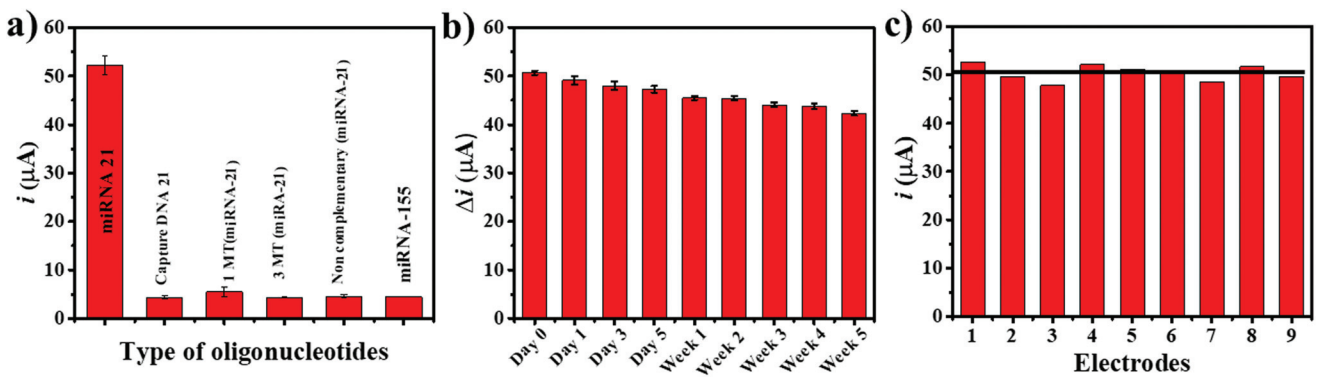

Fig. 9 (a) The responses of the DNA probe immobilized AuNPs/GP/PPY/SPCE toward 100 pM miRNA-21 and four oligonucleotide interferences (1 MT, 3 MT, non-complementary miRNA-21, and miRNA-155), (b) the stability test over five weeks, and (c) signals of nine electrodes in the detection of 100 pM miRNA-21.

miRNA-21 biosensor shows acceptable and good reproducibility (Fig. 9(c)).

Conclusions

A label-free electrochemical miRNA-21 biosensor using highly dispersed AuNPs-DNA-21 conjugates, a GP/PPY composite as a sensing support material, and MB as a signal probe is successfully developed. High particle dispersibility of AuNPs on a GP/PPY platform is observed, thus giving the high distribution of the DNA-21 probe and offering good properties of our biosensor. The redox current of MB distinctly increases only in the presence of the miRNA-21 target due to the formation of the double-stranded miRNA-21/DNA-21 complex. The prepared GP/PPY nanocomposite can increase both the surface area and conductivity of the electrode. The proposed electrochemical biosensor provides good sensitivity for the detection of miRNA-21 with a linear dynamic range from 0.0010 pM to 1.0 nM, a LOQ of 0.66 fM, and a LOD of 0.020 fM. The biosensor is demonstrated with high selectivity and reproducibility, which has a promising capability for the miRNA-21 assay in real serum samples. The sensor also gives acceptable long-term stability. In addition, this biosensor could be further developed for the detection of other miRNAs which are cancer biomarkers.

Author contributions

Chammari Pothipor: Investigation, result analysis, writing – original draft. Noppadol Aroonyadet: Conceptualization. Suwussa Bamrungsap: Writing – review and Editing. Jaroon Jakmunee: Writing – review and editing. Kontad Ounnunkad: Conceptualization, methodology, validation, resources, writing – original draft, writing – review & editing, visualization, supervision, project administration, and funding acquisition.

Conflicts of interest

There are no conflicts to declare.

Acknowledgements

This work was supported by Chiang Mai University (CMU) and CMU Mid-Career Research Fellowship program. C. P. would like to acknowledge an award of the Thailand Graduate Institute of Science and Technology (TGIST) 2017 (Grant No. TG-55-10-60-025D), and National Science and Technology Development Agency (NSTDA), Thailand. The authors gratefully acknowledge the Graduate School (CMU), Research Center on Chemistry for Development of Health Promoting Products from Northern Resources, Center of Excellence for Innovation in Chemistry (PERCH-CIC), Center of Excellence in Materials Science and Technology, and Department of Chemistry, Faculty of Science, CMU. The authors acknowledge financial support from Basic Research Fund, Thailand Science Research and Innovation (TSRI), Chiang Mai University (CMU).

References

1 A. Abrahamsson and C. Dabrosin, *Oncotarget*, 2015, **6**, 22959–22969.
2 O. Rehman, H. Zhuang, A. M. Ali, A. Ibrahim and Z. Li, *Cancers*, 2019, **11**, 431.
3 H.-A. Rafiee-Pour, M. Behpour and M. Keshavarz, *Biosens. Bioelectron.*, 2016, **77**, 202–207.
4 C. Catalanotto, C. Cogoni and G. Zardo, *Int. J. Mol. Sci.*, 2016, **17**, 1712.
5 Y. Peng and C. M. Croce, *Signal Transduction Targeted Ther.*, 2016, **1**, 15004.
6 W. Tan, B. Liu, S. Qu, G. Liang, W. Luo and C. Gong, *Oncol. Lett.*, 2018, **15**, 2735–2742.
7 H. Wang, R. Peng, J. Wang, Z. Qin and L. Xue, *Clin. Epigenet.*, 2018, **10**, 59.
8 J. Zhang and X. Hun, *Microchem. J.*, 2019, **150**, 104095.
9 M. Keshavarz, M. Behpour and H.-A. Rafiee-pour, *RSC Adv.*, 2015, **5**, 35651–35660.
10 F. Chen, F. Zhang, Y. Liu and C. Cai, *Talanta*, 2018, **186**, 473–480.
11 K. Asakura, T. Kadota, J. Matsuzaki, Y. Yoshida, Y. Yamamoto, K. Nakagawa, S. Takizawa, Y. Aoki, E. Nakamura, J. Miura, H. Sakamoto, K. Kato, S.-i. Watanabe and T. Ochiya, *Commun. Biol.*, 2020, **3**, 134.
12 J. Encarnación-Medina, C. Ortiz, R. Vergne, L. Padilla and J. Matta, *J. Oncol.*, 2019, **2019**, 14.
13 W. Wang and Y.-p. Luo, *J. Zhejiang Univ., Sci., B*, 2015, **16**, 18–31.
14 A. M. Grimaldi and M. Incoronato, *Cancers*, 2019, **11**, 901.
15 W. Zheng, J. Zhao, Y. Tao, M. Guo, Z. Ya, C. Chen, N. Qin, J. Zheng, J. Luo and L. Xu, *Oncol. Lett.*, 2018, **16**, 2777–2782.
16 J. Qu, J. Yang, M. Chen, L. Cui, T. Wang, W. Gao, J. Tian and R. Wei, *Pak. J. Med. Sci.*, 2019, **35**, 1466–1471.
17 H.-P. Tsai, S.-F. Huang, C.-F. Li, H.-T. Chien and S.-C. Chen, *PLoS One*, 2018, **13**, e0191195–e0191195.
18 F. Liang, M. Yang, N. Tong, J. Fang, Y. Pan, J. Li and X. Zhang, *Oncol. Lett.*, 2018, **16**, 4159–4168.
19 R. Hamam, A. M. Ali, K. A. Alsaleh, M. Kassem, M. Alfayez, A. Aldahmash and N. M. Alajez, *Sci. Rep.*, 2016, **6**, 25997.
20 S. Campuzano, M. Pedrero and J. M. Pingarrón, *Sensors*, 2017, **17**, 1993.
21 S. Campuzano, P. Yáñez-Sedeño and J. M. Pingarrón, *Sensors*, 2017, **17**, 866.
22 L. Tian, K. Qian, J. Qi, Q. Liu, C. Yao, W. Song and Y. Wang, *Biosens. Bioelectron.*, 2018, **99**, 564–570.
23 J. I. A. Rashid and N. A. Yusof, *Sensing and Bio-Sensing Research*, 2017, **16**, 19–31.
24 Y. Ren, H. Deng, W. Shen and Z. Gao, *Anal. Chem.*, 2013, **85**, 4784–4789.

25 T. Kangkamano, A. Numnuam, W. Limbut, P. Kanatharana, T. Vilaivan and P. Thavarungkul, *Biosens. Bioelectron.*, 2018, **102**, 217–225.
26 R. Salahandish, A. Ghaffarinejad, E. Omidinia, H. Zargartalebi, K. Majidzadeh-A, S. M. Naghib and A. Sanati-Nezhad, *Biosens. Bioelectron.*, 2018, **120**, 129–136.
27 P. Kara, K. Kerman, D. Ozkan, B. Meric, A. Erdem, Z. Ozkan and M. Ozsoz, *Electrochem. Commun.*, 2002, **4**, 705–709.
28 M. Liu, C. Luo and H. Peng, *Talanta*, 2012, **88**, 216–221.
29 L. Zhu, R. Zhao, K. Wang, H. Xiang, Z. Shang and W. Sun, *Sensors*, 2008, **8**, 5649–5660.
30 S. Han, W. Liu, S. Yang and R. Wang, *ACS Omega*, 2019, **4**, 11025–11031.
31 M. Holzinger, A. Le Goff and S. Cosnier, *Front. Chem.*, 2014, **2**, 63–63.
32 A. A. Jamali, M. Pourhassan-Moghaddam, J. E. N. Dolatabadi and Y. Omidi, *TrAC, Trends Anal. Chem.*, 2014, **55**, 24–42.
33 C. I. L. Justino, A. R. Gomes, A. C. Freitas, A. C. Duarte and T. A. P. Rocha-Santos, *TrAC, Trends Anal. Chem.*, 2017, **91**, 53–66.
34 H. V. Tran, B. Piro, S. Reisberg, L. D. Tran, H. T. Duc and M. C. Pham, *Biosens. Bioelectron.*, 2013, **49**, 164–169.
35 M. Zhou, M. Pagels, B. Geschke and J. Heinze, *J. Phys. Chem. B*, 2002, **106**, 10065–10073.
36 Y. Xu, X. Ye, L. Yang, P. He and Y. Fang, *Electroanalysis*, 2006, **18**, 1471–1478.
37 A. Yussuf, M. Al-Saleh, S. Al-Enezi and G. Abraham, *Int. J. Polym. Sci.*, 2018, **2018**, 4191747.
38 P. Wang, Y. Zheng and B. Li, *Synth. Met.*, 2013, **166**, 33–39.
39 J. Wang and N. Hui, *Sens. Actuators, B*, 2019, **281**, 478–485.
40 J. Galandová and J. Labuda, *Chem. Pap.*, 2008, **63**, 1.
41 T. Qian, C. Yu, X. Zhou, S. Wu and J. Shen, *Sens. Actuators, B*, 2014, **193**, 759–763.
42 H. Mao, J. Liang, H. Zhang, Q. Pei, D. Liu, S. Wu, Y. Zhang and X.-M. Song, *Biosens. Bioelectron.*, 2015, **70**, 289–298.
43 S. K. Krishnan, E. Singh, P. Singh, M. Meyyappan and H. S. Nalwa, *RSC Adv.*, 2019, **9**, 8778–8881.
44 F. Li, Y. Zhou, H. Yin and S. Ai, *Biosens. Bioelectron.*, 2020, **166**, 112476.
45 S. A. Bhat, S. A. Pandit, M. A. Rather, G. M. Rather, N. Rashid, P. P. Ingole and M. A. Bhat, *New J. Chem.*, 2017, **41**, 8347–8358.
46 Y. F. Wu, Y. Yao, S. Cheong, R. D. Tilley and J. J. Gooding, *Chem. Sci.*, 2020, **11**, 12570–12579.
47 R. Tavallaie, J. McCarroll, M. Le Grand, N. Ariotti, W. Schuhmann, E. Bakker, R. D. Tilley, D. B. Hibbert, M. Kavallaris and J. J. Gooding, *Nat. Nanotechnol.*, 2018, **13**, 1066.
48 J. J. Gooding and V. R. Goncales, *Curr. Opin. Electrochem.*, 2017, **5**, 203–210.
49 F. Malvano, D. Albanese, A. Crescitelli, R. Pilloton and E. Esposito, *Biosensors*, 2016, **6**, 33.
50 B. Hao, T. Song, M. Ye, X. Liu, J. Qiu, X. Huang, G. Lu and W. Qian, *Biomater. Sci.*, 2020, **8**, 6037–6044.
51 Y.-H. Wang, L.-L. He, K.-J. Huang, Y.-X. Chen, S.-Y. Wang, Z.-H. Liu and D. Li, *Analyst*, 2019, **144**, 2849–2866.
52 X. He, W. Liu, X. Zhang, X. Zhang and J. Chen, *Anal. Methods*, 2014, **6**, 6893–6899.
53 E. Liu and X. Zhang, *Anal. Methods*, 2014, **6**, 8604–8612.
54 A. A. Volkert, V. Subramaniam, M. R. Ivanov, A. M. Goodman and A. J. Haes, *ACS Nano*, 2011, **5**, 4570–4580.
55 L. Zhang, X. Li, Y. Huang, Y. Ma, X. Wan and Y. Chen, *Carbon*, 2010, **48**, 2367–2371.
56 H. A. Becerril, J. Mao, Z. Liu, R. M. Stoltenberg, Z. Bao and Y. Chen, *ACS Nano*, 2008, **2**, 463–470.
57 C. Pothipor, N. Kungwan, J. Jakmunee and K. Ounnunkad, *Chem. Lett.*, 2015, **44**, 800–802.
58 H. C. Kang and K. E. Geckeler, *Polymer*, 2000, **41**, 6931–6934.
59 A. Ambrosi, C. K. Chua, N. M. Latiff, A. H. Loo, C. H. A. Wong, A. Y. S. Eng, A. Bonanni and M. Pumera, *Chem. Soc. Rev.*, 2016, **45**, 2458–2493.
60 L. Liu, G. Zhao, X. Dong, X. Li, Q. Wei and W. Cao, *Anal. Methods*, 2018, **10**, 4917–4925.
61 R. Wang and C. Xue, *Anal. Methods*, 2013, **5**, 5195–5200.
62 R. Tavallaie, N. Darwish, M. Gebala, D. B. Hibbert and J. J. Gooding, *ChemElectroChem*, 2014, **1**, 165–171.
63 S. M. Silva, S. Hoque, V. R. Gonçales and J. J. Gooding, *Electroanalysis*, 2018, **30**, 1529–1535.
64 D. Pan, X. Zuo, Y. Wan, L. Wang, J. Zhang, S. Song and C. Fan, *Sensors*, 2007, **7**, 2671–2680.
65 J. Wang, J. Lu, S. Dong, N. Zhu, E. Gyimah, K. Wang, Y. Li and Z. Zhang, *Biosens. Bioelectron.*, 2019, **130**, 81–87.
66 Q. Xiao, J. Li, X. Jin, Y. Liu and S. Huang, *Sens. Actuators, B*, 2019, **297**, 126740.
67 A. F.-J. Jou, Y.-J. Chen, Y. Li, Y.-F. Chang, J.-j. Lee, A. T. Liao and J.-a. A. Ho, *Electrochim. Acta*, 2017, **236**, 190–197.
68 N. Xia, Y. Zhang, X. Wei, Y. Huang and L. Liu, *Anal. Chim. Acta*, 2015, **878**, 95–101.
69 T. Kilic, S. N. Topkaya, D. Ozkan Ariksoysal, M. Ozsoz, P. Ballar, Y. Erac and O. Gozen, *Biosens. Bioelectron.*, 2012, **38**, 195–201.
70 M. Kaplan, T. Kilic, G. Guler, J. Mandli, A. Amine and M. Ozsoz, *Biosens. Bioelectron.*, 2017, **92**, 770–778.
71 H. Yin, Y. Zhou, H. Zhang, X. Meng and S. Ai, *Biosens. Bioelectron.*, 2012, **33**, 247–253.
72 C.-Y. Hong, X. Chen, T. Liu, J. Li, H.-H. Yang, J.-H. Chen and G.-N. Chen, *Biosens. Bioelectron.*, 2013, **50**, 132–136.

